This is the accepted version of an article pubbished in Journal of the Mechanical Behavior of Biomedical Materials, Volume 104, April 2020, 103656. The final publication is available at https://dx.doi.org/10.1016/j.jmbbm.2020.103656

Mechanical properties of diamond lattice Ti-6Al-4V structures produced by laser powder bed fusion: on the effect of the load direction

Antonio Cutolo[a,*], Bert Engelen[b], Wim Desmet[a,c], Brecht Van Hooreweder[a,d]

[a] *KU Leuven Department of Mechanical Engineering, Celestijnenlaan 300, 3001 Leuven (Heverlee), Belgium*
[b] *3DSystems Leuven, Grauwmeer 14, B-3001 Leuven, Belgium*
[c] *DMMS Core Lab, Flanders Make, 3001 Leuven (Heverlee), Belgium*
[d] *Members Flanders Make, Leuven, Belgium*

Abstract

Laser powder bed fusion (L-PBF) techniques have been increasingly adopted for the production of highly personalized and customized lightweight structures and bio-medical implants. L-PBF can be used with a multiplicity of materials including several grades of titanium. Due to its biocompatibility, corrosion resistance and low density-to-strength ratio, Ti-6Al-4V is one of the most widely used titanium alloys to be processed via L-PBF for the production of orthopedic implants and lightweight structures.

Mechanical properties of L-PBF Ti-6Al-4V lattice structures have mostly been studied in uniaxial compression and lately, also in tension. However, in real-life applications, orthopedic implants or lightweight structures in general are subjected to more complex stress conditions and the load directions can be different from the principal axes of the unit cell.

In this research, the mechanical behavior of Ti-6Al-4V diamond based lattice structures produced by L-PBF is investigated exploring the energy absorption and failure modes of these metamaterials when the loading directions are different from the principal axis of the unit cell. Moreover, the impact of a heat treatment (i.e. hot isostatic pressing) on the mechanical properties of the aforementioned lattice structures has been evaluated. Results indicate that the mechanical response of the lattice structures is significantly influenced by the direction of the applied load with respect to the unit cell reference system revealing the anisotropic behavior of the diamond unit cell.

Keywords: laser powder bed fusion - Ti-6Al-4V - lattice structures - anisotropy

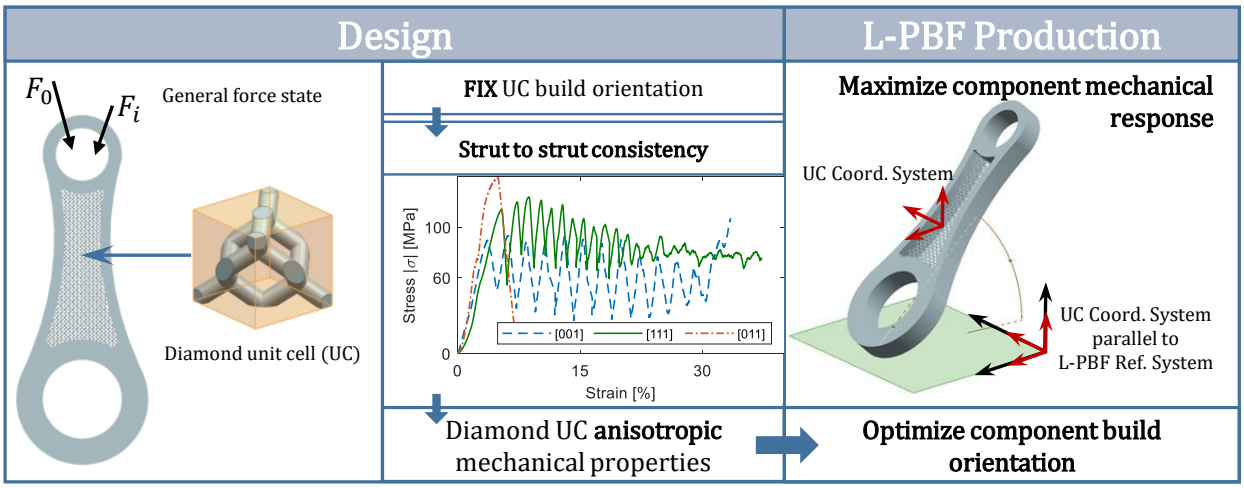

1. Introduction

Due to its high strength-to-density ratio, corrosion resistance and biocompability [1], Ti-6Al-4V is one of the most widely used materials for lightweight structures and bio-medical implants. Given the high costs related to material removal arising from conventional manufacturing techniques, several industrial areas are considering more and more additive manufacturing (AM) techniques for Ti-6Al-4V components production [2, 3].

Laser powder bed fusion (L-PBF) is an AM technique that uses a focused and computer controlled laser to selectively melt metal powder in order to produce components, layer by layer, directly from CAD representations. This technique allows the production, with efficient material use, of complex net-shape geometry including porous structures also called scaffolds or lattice structures.

Lattice structures are a particular class of cellular solids comprising nodes connected by beam-like members, named struts. They can be classified in bending dominated and stretching dominated structures, according to Maxwell's stability criterion [4]. Stretching dominated structures exhibit higher stiffness and strength, whereas bending dominated structures possess better energy absorption properties because of a longer plateau stress when undergoing compressive loads [5, 6, 7]. Lattice structures are gathering more and more interest from different industrial areas, such as biomedical and aerospace industry, since they are suited for both weight reduction and mechanical properties tailoring.

The mechanical properties of lattice structures are widely studied and are affected by several variables such as unit cell architecture, relative density, parent material, etc [8, 9, 10, 11]. Beside these variables, production parameters and post-production operations can provide beneficial effects on the mechanical response of these structures [12, 13, 14].

The design of the unit cell is a critical phase in the AM work-flow since it can severely impact the mechanical properties of the final lattice structure. In particular for L-PBF part production, overhang structures or members with small inclination with respect to the build platform should be avoided [15, 16, 17] since they can be affected by severe dross formation that can be detrimental for the structural integrity of the final part. Therefore, when designing the unit cell architecture and conceiving its orientation with respect to the build platform, horizontal struts are to be avoided.

In general, different design approaches can be used to tune the mechanical properties of porous lattice structures within one larger component such as a biomedical implant. A local variation in stiffness and/or strength, or a certain anisotropy within one lattice structure can be required based on the specific application and load cases. One design approach could be to use different unit cell types in one lattice structure, or to change the unit cell orientation with respect to the base plate to favor properties in particular locations/directions. The disadvantages of that approach are the typically weak interfaces between different types of unit cells and the variability in strut geometries/properties when different strut-to-baseplate orientations are used in one sample. Another, more favorable approach could therefore be to use a fixed unit cell orientation compared to the base plate and to orient the component's geometry in a way that the anisotropic unit cell behavior is taken into account.

As far as the authors know, only a limited number of studies has been conducted to evaluate if a different loading direction can have effect on mechanical properties of lattice structures. Xu et al. [18] proposed a numerical methodology to evaluate the anisotropy of unit cells based on the homogenization method [19]. From an experimental point of view, Wauthle et al. [20] explored the effect of build orientation on microstructure and compressive mechanical properties of additively manufactured Ti-6Al-4V lattice structures concluding that the diamond unit cell can be considered isotropic since the effect of the unit cell orientation cannot be distinguished in the mechanical properties. A similar study but with different results, was conducted by Soul et al. [21] in which the mechanical behavior of Al-Si-10Mg lattice structures has been evaluated. In particular, Soul et al. reported a significant impact of the diamond unit cell orientation with respect to the loading direction on the mechanical properties both in monotonic and cyclic conditions. Lietaert et al. [22] focused on quasi-static and fatigue properties of Ti-6Al-4V diamond lattice structures undergoing compressive and tensile stresses reporting an axial isotropic behavior of the diamond unit cell in terms of static properties. Lietaert et al. also reported a dependence of the fatigue performances with respect to the load direction. However, none of these studies included an investigation on the failure modes and energy absorption of the diamond unit cell for loading directions that are different form the principal axes of the unit cell.

*Corresponding author
Email address: antonio.cutolo@kuleuven.be (Antonio Cutolo)
URL: www.set.kuleuven.be/am/ (Antonio Cutolo)

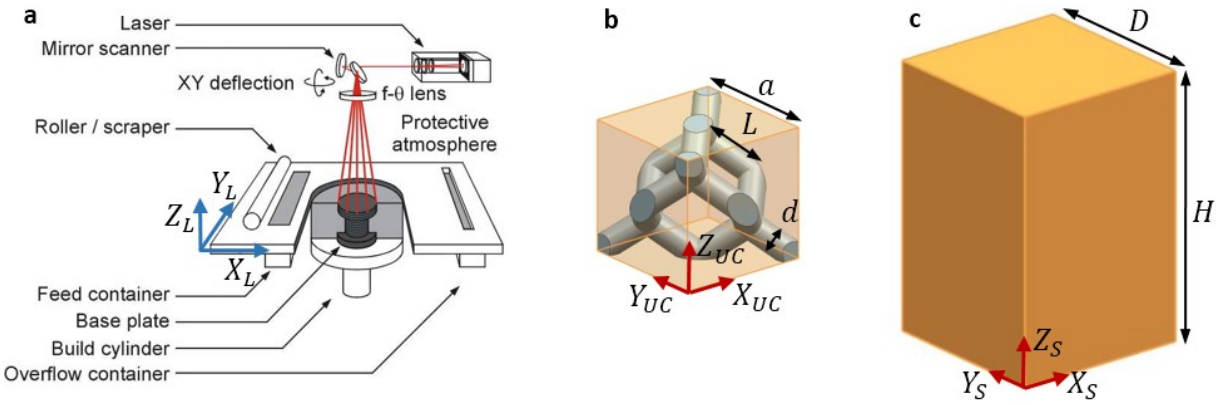

Figure 1: a) L-PBF reference coordinate system; b) Diamond unit-cell coordinate system; c) Sample coordinate system

The present study investigates the influence of the load direction with respect to the unit cell orientation on the mechanical properties of Ti-6Al-4V diamond based lattice structures produced by L-PBF. In particular, an extensive experimental campaign is conducted by means of compressive quasi-static tests to assess if mechanical properties are affected by changing the load direction with respect to the unit cell coordinate system. Moreover, the failure mechanism of these structure has been investigated both on a macro level and on a micro level. Finally, the effect of hot isostatic pressing (HIP) on the mechanical properties, failure mechanism and energy absorption is determined.

The final purpose of this study is to provide design guidelines for using lattice structures in load bearing applications subjected to a well known load environment. The results of this study show that it is possible to improve the mechanical response of the meta-material under investigation by changing the lattice unit cell orientation with respect to the load direction without changing mass and relative density of the structure. The change in orientation can be obtained by rotating the geometry under investigation, with respect to the L-PBF built plate with a fixed orientation between the unit cell and the build plate. As a result the production of horizontal members can be avoided.

This information can be used in the design stage of the AM work-flow for optimizing the part orientation with respect to the built chamber in order to maximize the mechanical response of the structure. Moreover, by using a similar approach the energy absorption can be improved for a specific angle between the load and the unit cell orientation.

2. Materials and Methods

2.1. Sample design and production

For this investigation, a diamond cell geometry is used for the generation of the lattice structures. This unit cell can be described as a spatial arrangement of nodes connected by struts of length L and diameter d, as shown in Figure 1b, with an angle of 109.48° between every pair of struts connected by one node. One of the advantages of using this geometry is that the angle between the struts and the horizontal plane X_{UC}, Y_{UC} is 35.26°. This angle is high enough for production of these structures via L-PBF avoiding the use of support structures [23]. In fact, since all struts have the same inclination with the X_L, Y_L plane, the L-PBF technique can ensure strut-to-strut consistency in terms of strut diameter, strut length and surface roughness. Therefore, when fixing this unit cell orientation it can be assumed that all the struts in each unit cell of the lattice structure exhibits same mechanical response. For every other orientation of the unit cell with respect to the L-PBF reference system the production process will introduce additional ”anisotropy” depending on variation in struts diameter and surface roughness induced by the L-PBF process. For these reasons, all the samples produced by means of L-PBF in this investigation were designed with a fixed orientation between the unit cell and the build platform.

The samples used for this study are prisms with a square cross-section, a side D of 10mm and a height H of 15mm (Figure 1-c). The unit cell side a is 1mm with a relative density of 25%. In this case, the strut length L is equal

to 0.43mm and the strut diameter d is 0.24mm. The dimensions L and d have been evaluated using the analytical formulation developed by Gibson et al. [6, 12].

In order to obtain different orientations between the load direction and the unit cell, the specimens were produced with different orientations compared to the build plane of the L-PBF machine (i.e. X_L, Y_L) while maintaining fixed the unit cell orientation. Three coordinate systems were considered: the L-PBF reference coordinate system (X_L, Y_L, Z_L) with layers being deposed in the X_L, Y_L plane (Figure 1-a), the unit cell coordinate system (X_{UC}, Y_{UC}, Z_{UC}) with its axis along the ribs of the cube in which the unit cell is inscribed (Figure 1-b), and the sample coordinate system with the axis (X_S, Y_S, Z_S) along the ribs of the cuboids of Figure 1-c. During the production of the specimens, the L-PBF and unit cell coordinate systems were parallel, while the sample coordinate system has been rotated with respect to the L-PBF reference coordinate system. In particular, three different sample orientations were considered indicated as [001], [111] and [011]. The [001] orientation was obtained with X_L, Y_L, Z_L parallel to X_S, Y_S, Z_S (Figure 2-a). In order to obtain [111] orientation X_S, Z_S and Y_S, Z_S planes were both placed at 54.74° inclination with respect to X_L, Y_L (Figure 2-b). The [011] orientation was obtained by rotating X_S, Z_S and Y_S, Z_S planes of of 45° with respect to X_L, Y_L plane (as indicated in Figure 2-c); in this case the Z_S axis is aligned with the X_L, Y_L plane. The Miller index notation is used to indicate load direction with respect to the unit cell reference system (Figure 2-d-e-f).

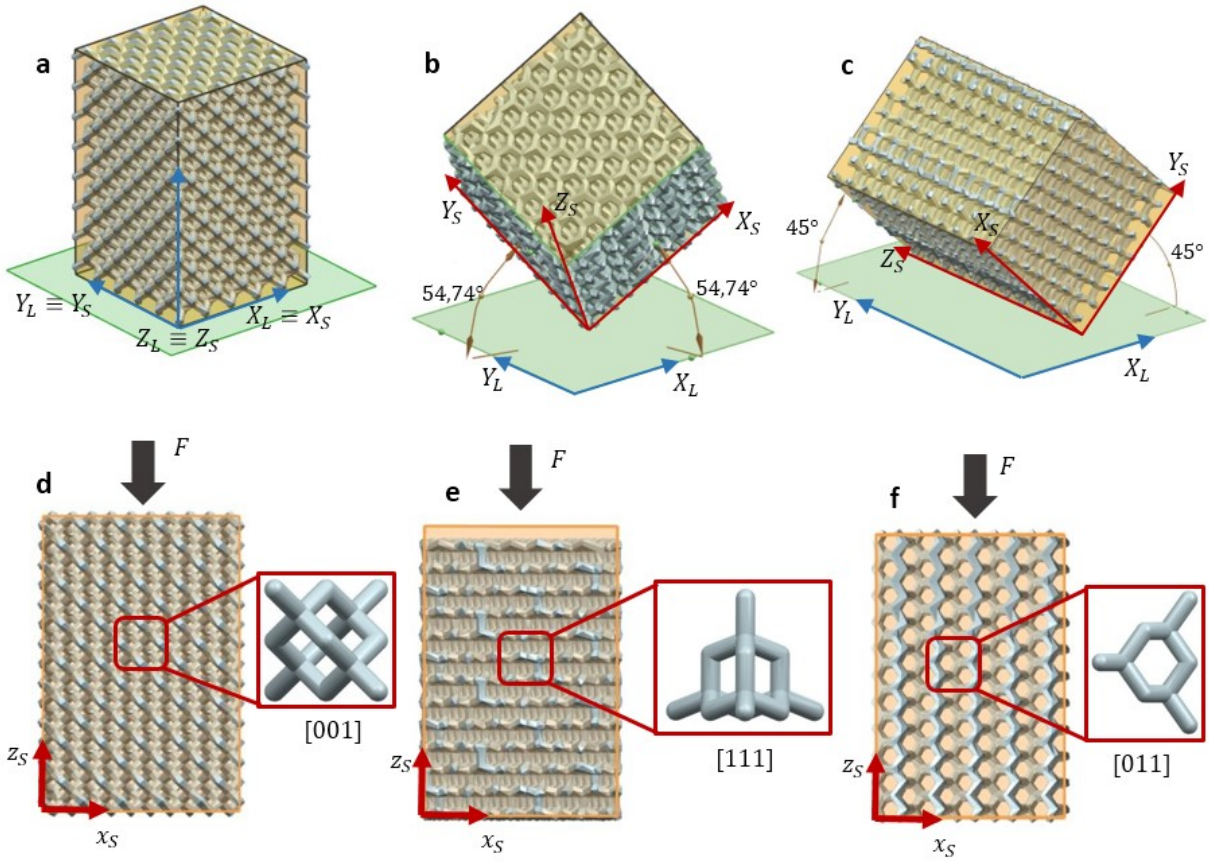

Figure 2: Sample orientation with respect to the build plate: a) [001] orientation, b) [111] orientation and c) [011] orientation Force direction with respect the sample reference systems and the unit cell for d) [001] orientation, e) [111] orientation and f) [011] orientation

Samples were produced via L-PBF on a ProX DMP 320 machine using 3D Systems optimized process parameters from LaserForm Ti Gr.23 powder (ASTM F3001 standard). The samples were produced with a layer thickness of 30μm on a Ti base plate and support structures were used for [111] and [011] oriented samples. The input CAD file for the three different orientations had a relative density of 25%.

For each of the three different orientations, 10 samples were produced, of which 5 were subjected to hot isostatic

pressing post-treatment (HIP). This treatment consists of heating the samples to a temperature of $920°C$ and a pressure of $1000bar$ for $2h$. This treatment has been extensively used on Ti-6Al-4V produced by L-PBF for closing residual pores generated during the manufacturing process [24], for releaving potential residual stresses and to produce a change in microstructure that enhances the ductility of this alloy [25].

2.2. Sample characterization and mechanical testing

For each sample produced, the strut density ρ_{strut} and the relative density ρ_{rel} (volume of the structure divided by the volume of the prisms) of the samples were determined. The mass was measured with a O'Haus Pioneer balance with accuracy of $0.1mg$ equipped with a calibrated O'Haus Archimede's kit. The volume was calculated from the height H and the side D measured with a digital caliper with $0.01mm$ resolution. The strut density was calculated by measuring dry-mass and submerged-mass in ethanol. Based on these measurements and on the Ti-6Al-4V theoretical density ($4.42g/cm^3$), ρ_{strut} and the relative density ρ_{rel} were calculated [26, 27].

One representative sample for as-built and HIP condition was ground and polished for optical microscopy with a Keyence VHX-6000. A 2% HF solution was used to etch Ti-6Al-4V samples to detect possible α case if present. Quasi-static uniaxial compression tests were performed on an Instron 3360 equipped with a $30kN$ force cell according to ISO 13314 [28]. For the mechanical tests a constant displacement rate of $0.9mm/min$ was used. Teflon sheets, with a thickness of $0.2mm$, were used as solid lubricant between the samples and the compression plates to reduce the development of elevate lateral friction forces that could lead to barreling of the sample during the compression test. At least 3 samples were tested for every condition. The strain was measured using a Instron Video Extensometer AVE2. The distance between the two compression plates was considered as gage length. Tests were stopped when a drop of 80% of the force occurred. The applied loads were used to evaluate the apparent stress in the structure dividing the applied force value by the sample cross sectional area along the (X_S, Y_S) plane, $\sigma = \frac{F}{D^2}$, in which F is the applied force and D is the side dimension of the sample. The side dimension D was measured for each sample using a digital caliper with $0.01mm$ resolution.

Every test was recorded with two digital cameras equipped with $12M - pixels$ sensor to monitor deformations and failure modes of the lattice structures.

For every test the following properties were evaluated: compressive stress σ, compressive strain ϵ, quasi-elastic gradient, first maximum stress and its corresponding strain and the energy absorption W using the relation expressed in equation 1.

$$W = \frac{1}{100} \int_0^{\epsilon_0} \sigma(\epsilon) d\epsilon \tag{1}$$

For [001] and [111] orientation the value of the energy absorption was evaluated between 0 and 30% of the strain, whilst for [011] orientation this quantity was evaluated until the complete failure of the structure. It is important to remark that the stresses calculated in this research refer to apparent stresses acting on the lattice structure i.e. the applied load divided by the cross sectional area of the cuboids. An approximation of the stress in the struts of the samples has been provided by Van Hooreweder et al. [12] but this has not been used in this investigation.

After mechanical testing, fractured samples were analyzed via scanning electron microscope (SEM) using a XL30 FEG.

3. Results

As reported in Table 1, the strut density measured on the as-built samples is higher than 98.50%. After HIP treatment, the residual porosity decreased and the measured strut density was systematically higher than 99.40%. These results were qualitatively confirmed by Figure 3 in which representative cross-sections of as-built and HIP'ed samples are presented. It is clearly visible how in the as-built sample (Figure 3-a) large pores generated during the manufacturing process are visible while these pores are almost eliminated after the HIP treatment (Figure 3-b).

The results of quasi-static compression tests in terms of averages and standard deviations are reported in Table 1 and in Figure 4, Figure 5 and Figure 6 representative stress-strain curves are reported. In Table 2, Table 3 and Table 4 representative failure modes of the three different orientations are shown for as-built and HIP condition.

Specimens for the [001] orientation exhibit a lower quasi-elastic gradient and first maximum stress in both as-built and HIP'ed condition when compared to [011] and [111] orientations. This observation indicates the anisotropic behavior of the diamond unit cell when compared with cubic symmetry crystals.

Table 1: Sample mass, densities and mechanical properties for [001], [111] and [011] in as-built and HIP'ed condition

Condition	as built (ASB)			HIP		
Orientation	[001]	[111]	[011]	[001]	[111]	[011]
Mass [g]	2.27 ± 0.06	2.3 ± 0.06	2.25 ± 0.06	2.33 ± 0.02	2.28 ± 0.07	2.23 ± 0.07
Relative density [%]	31.92 ± 0.80	30.09 ± 0.76	31.06 ± 0.93	33.24 ± 0.32	32.71 ± 0.85	30.85 ± 0.76
Strut's density [%]	98.69 ± 0.10	98.61 ± 0.19	98.76 ± 0.10	99.50 ± 0.16	99.48 ± 0.85	99.63 ± 0.76
Quasi elastic gradient [GPa]	3.38 ± 0.13	3.85 ± 0.19	5.40 ± 0.46	3.26 ± 0.16	4.36 ± 0.44	5.24 ± 0.71
First maximum stress [MPa]	91.24 ± 8.23	114.94 ± 2.37	133.30 ± 9.35	98.49 ± 1.88	133.68 ± 7.19	133.94 ± 10.56
Strain at maximum stress [%]	4.33 ± 0.14	5.40 ± 0.02	4.79 ± 0.19	6.68 ± 0.13	7.80 ± 0.99	8.54 ± 0.23
Energy absorption (30% strain) $[MJ/m^3]$	17.53 ± 2.49	25.30 ± 3.8	-	22.71 ± 1.88	27.47 ± 4.10	-
Energy absorption (before failure [011] orientation) $[MJ/m^3]$	-	-	5.41 ± 1.02	-	-	7.51 ± 0.85

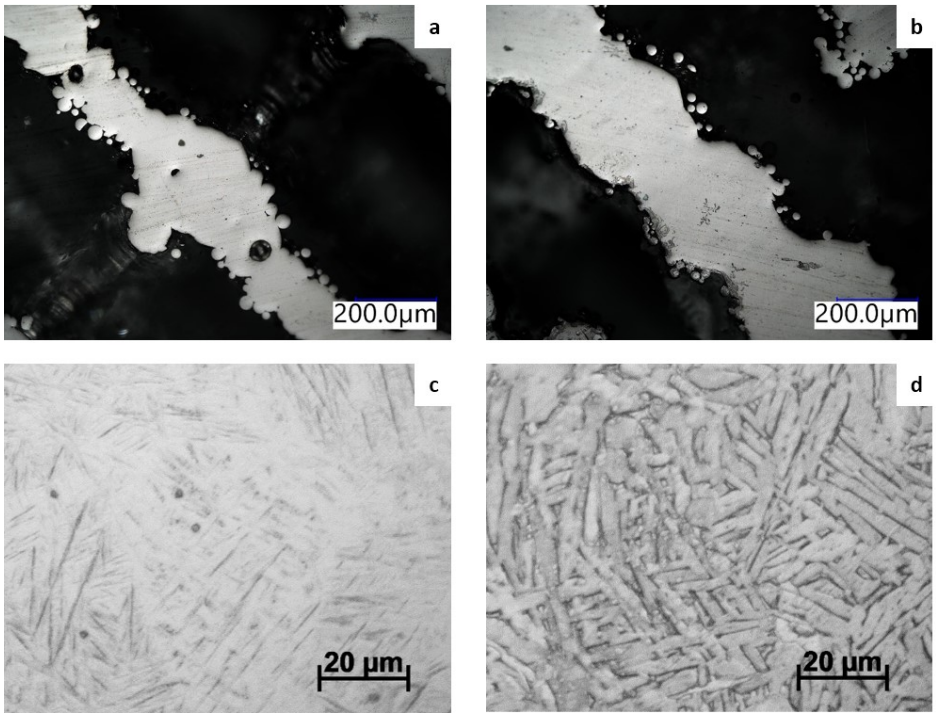

Figure 3: Optical microscope pictures of transverse cross-section for as-built sample (a) and HIP'ed sample (b); microstructure for Ti-6Al-4V in as-built (c) and HIP'ed condition. The building direction is perpendicular to the plane of the pictures

3.1. Microstructure evolution after HIP treatment

In as-built condition L-PBF Ti-6Al-4V exhibits an acicular martensitic microstructure with fine α' martensitic needles created by the rapid cooling rates generated in the L-PBF process [29]. After HIP post treatment, a coarse $\alpha + \beta$ microstructure is obtained from the decomposition of the α' needles. These two types of microstructures are clearly visible in Figure 3-c and Figure 3-d.

It is well documented in literature [25] that in as-built condition the martensitic Ti-6Al-4V microstructure can be considered as the cause for relatively high strength and low ductility. Subsequent to HIP treatment, the α' microstructure coarsens into a $\alpha + \beta$ lamellae that increases the ductility of the material. Higher ductility has been observed for all the three different batches ([001], [111] and [011]) that underwent HIP treatment, as reported in Table 1. In fact, the value of the strain at maximum stress systematically increased for [001], [111] and [011] orientations after the HIP treatment.

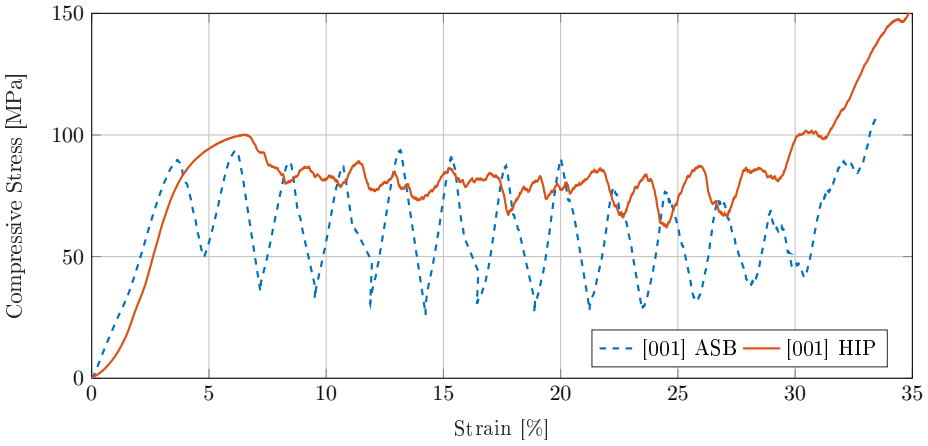

Figure 4: Stress-strain relation for [001] orientation in ASB and HIP'ed condition

3.2. Failure modes - Macro level

3.2.1. [001] orientation

In as-built condition, quasi-static data of the [001] orientation show linear behavior followed by oscillating stress-strain relation (Figure 4) which is the result of successive brittle failures of layers of unit cells oriented along a slip plane inclined by 54.74° with respect to the horizontal plane X_S, Y_S, as it can be observed in Figure 4 and Table 2 for 15% of the global strain. First the stress increases to a maximum at which one, or more, layers of unit cells fail. This is followed by a stress decrease that corresponds to the sudden brittle collapse of that layer. When large strain values are reached, [001] oriented samples show the typical stiffening behavior due to densification of the structure. This failure mode has been reported in literature by several authors [12, 30, 31].

For HIP'ed [001] specimens, the fluctuating stress behavior is much more damped (Figure 4) indicating that successive layers of struts were plastically deformed until the densification of the structure. The plastic deformation

Table 2: Failure modes for ASB and HIP [001] orientation for different values of the strain

Condition	Strain(ϵ, [%])				F direction VS UC
[001] ASB	0	10	15	32	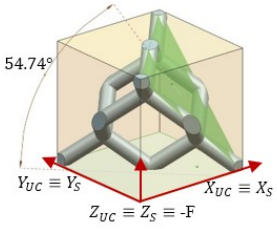
[001] HIP	0	7	25	32.5	

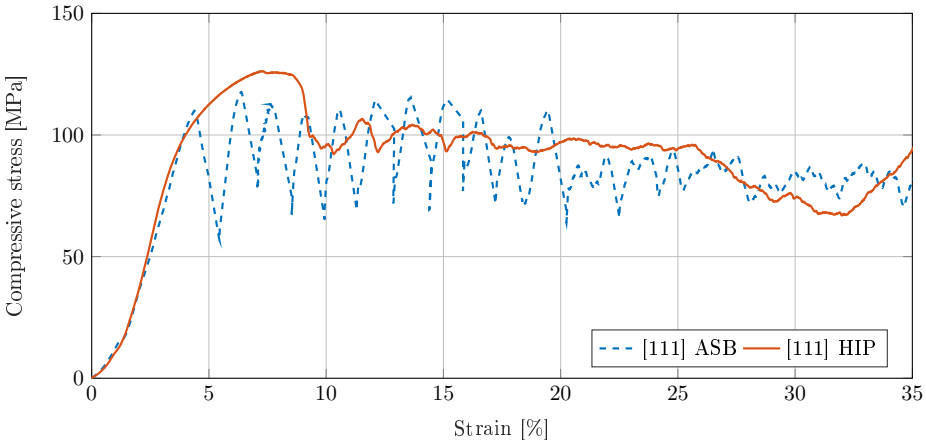

Figure 5: Stress-strain relation for [111] orientation in ASB and HIP'ed condition

occurred along a slip plane inclined by 54.74° with respect to the horizontal plane (X_S, Y_S) as illustrated in Table 2 for 7% of the global strain.

3.2.2. [111] orientation

As shown in Figure 5, the [111] oriented samples exhibit a similar type of failure mode when compared to [001] oriented samples. In as-built condition the initial linear behavior (Figure 5) is followed by successive brittle failures that occurred along planes with an inclination of 70.53° to the horizontal plane (Table 3) indicating that in this case the slip plane changes its orientation when the unit cell is rotated with respect to the loading direction. For the HIP'ed samples no brittle failures were recorded (Figure 5) and a well-defined plateau stress was observed. This behavior can be attributed to plastic deformation of layer of struts along planes inclined of 70.53° with respect to the horizontal plane as shown in Table 3 at 22.5% of the strain.

Table 3: Failure modes for ASB and HIP [111] orientation for different values of the strain

Condition	Strain(ϵ, [%])				F direction VS UC
[111] ASB	0	7.5	12.5	30	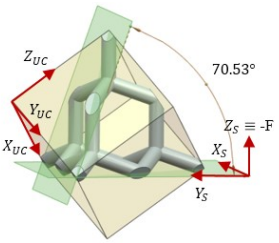
[111] HIP	0	12.5	22.5	32.5	

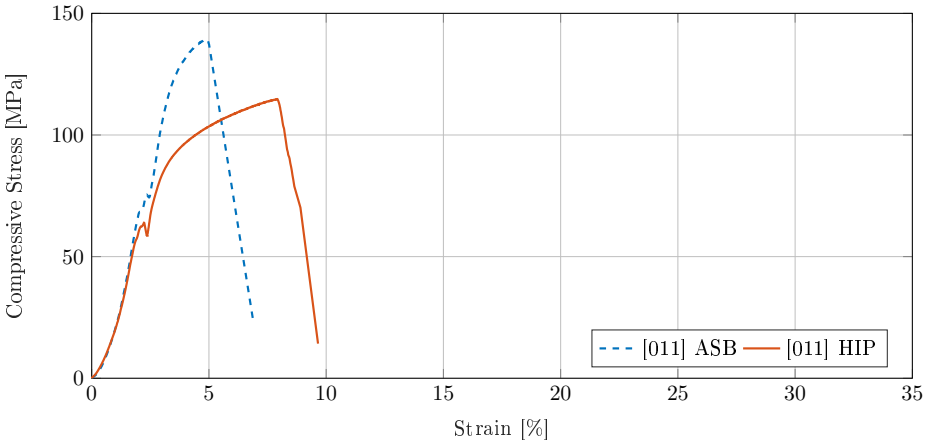

Figure 6: Stress-strain relation for [011] orientation in ASB and HIP'ed condition

3.2.3. [011] orientation

Another type of failure mode was observed for the [011] orientation. In this case the samples failed completely after the first maximum stress was reached in both as-built and HIP'ed condition with a single slip plane inclined by 35.23° with respect to the horizontal plane (Table 4). When the load direction is oriented as indicated in Figure 2-f, the lattice structure looses its ability to absorb energy, behaving in a similar way as a solid material under compression. In this case, all the struts along the slip plane failed simultaneously resulting in a complete fracture of the specimen that was not able to bear any further load.

3.3. Failure modes - Micro level

The characterization of the failure mechanisms on strut level has been performed by analyzing fractured strut surfaces via SEM. Representative fractured surfaces are presented in Figure 7 for as-built samples and in Figure 8 for HIP'ed specimens. From the analysis of SEM pictures, three different failure behaviors have been identified. The first failure type can be observed in Figure 7-a-d-b-e and Figure 8-a-d-b-e for [001] and [111] oriented samples in both

Table 4: Failure modes for ASB and HIP [011] orientation for different values of the strain

Condition	Strain(ϵ, [%])		F direction VS UC
[011] ASB	0	4.8	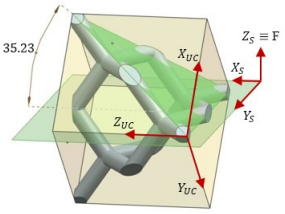
[011] HIP	0	8.3	

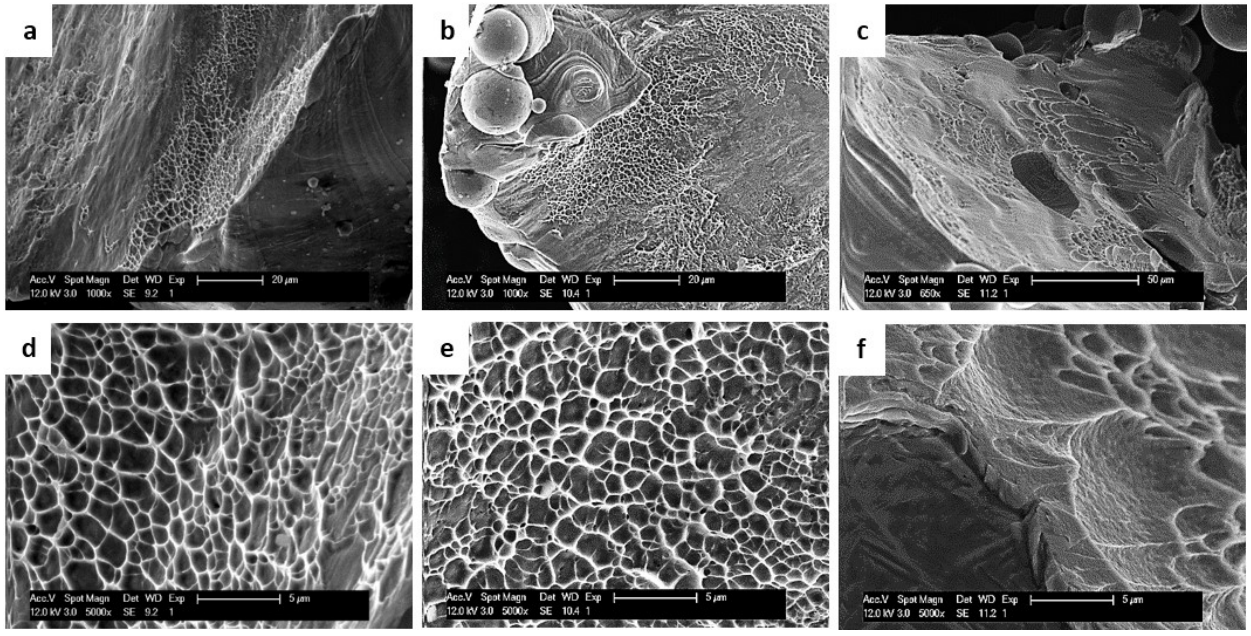

Figure 7: Representative fractured struts in as-built condition for: [001] orientation (a, d); [111] orientation (b, e); [011] orientation (c, f)

as-built and HIP'ed condition: it consists of dimple tearing rupture indicating a ductile type of fracture. In this case the dimple exhibit regular shapes and sizes in both as-built and HIP'ed condition. The second type of failure can be observed in Figure 7-a-d and Figure 8-a-d. It consists of smooth features indicating cleavage planes as sign of brittle failure. The third type of failure mechanism has been observed only for [011] samples, both in as-built and HIP'ed condition. In this case the fractured struts exhibit a different dimple morphology (Figure 7-c-f, Figure 8-c-f) with respect to the other samples showing a combination of regular sized dimple and elongated ones. This type of rupture is typical for shear stress based failure [32].

The combination of ductile dimple and cleavage fracture of Figure 7-a and Figure 7-b, related to [001] and [111] as-built samples, indicates a mixed mode of ductile and brittle failure. This combination of brittle and ductile failure mode has been reported by several studies on failure mechanism of Ti-6Al-4V lattice structures produced by AM techniques. Ataee et al. [33] addressed this failure mode behavior to the presence of large fraction of $\frac{\alpha'}{\alpha}$ phase in as-built condition as main responsible for the brittle type of failure. Similar results have been reported by Zhao et al. [34].

As far as the authors know, there are no studies on lattice structures in literature reporting similar behavior of [011] samples. In this case, fractography indicates the important role of shear stresses on producing elongated dimple morphology [32], suggesting that for [011] oriented specimens, the compressive load is redistributed as shear stresses on a local scale. In order to further characterize the local stress distribution across the struts for the three different sample sets, numerical simulation is needed.

3.4. Energy absorption

Table 1 reports the energy absorption of as-built and HIPed samples for [001] and [111] orientations up to 30% of the strain. Figure 9 shows the cumulative energy absorption per unit volume in function of the compressive strain for as-built and HIP'ed lattice structures for different load directions with respect to the unit cell.

In as-built condition the three different lattice structures considered (i.e. [001], [111] and [011]) exhibit different total energy absorption values with [111] samples having the highest value of energy absorption when 30% of the strain is considered (blue dashed curve in Figure 9). The results of [001] and [111] oriented samples show a slight oscillation of the cumulative energy absorption in function of the lattice strain (blue curves in Figure 9). The deviation from the ideal linear behavior can be attributed to successive brittle failures along diagonal shear bands corresponding to sudden high energy release [35]. The total energy absorbed by [011] samples is much lower with respect to the

other batches, since these samples failed completely after the first maximum compressive stress was reached. In this case the structure is only able to absorb energy for strain values lower than 5%.

In the case of HIP'ed samples, [111] samples present higher energy absorption values if compared to [001] samples at a strain of 30%. These values are also higher than the energy absorbed by as-built [001] and [111] samples, indicating that the change in microstructure induced by the HIP process enhances the ability of these structure to absorb energy. In fact, HIP'ed [001] and [111] samples do not present a fluctuating stress-strain behavior and their struts deform more plastically, preventing the release of energy generated by brittle failures, as is the case for as-built samples. The cumulative energy absorption behavior for HIP'ed samples in Figure 9 is approximately linear.

For [011] HIP'ed samples, the total absorbed energy is much lower than HIP'ed [001] and HIP'ed [111] samples due the structural collapse around 9% of the strain.

4. Discussion

The present study assesses the mechanical behavior of diamond based lattice structures in function of the load direction acting on the unit cell. In scientific literature, different opinions with respect to isotropic or anisotropic behavior of single crystal inspired lattice structures can be found.

On one side Wauthle et al. [20] concluded that there is no influence of the unit cell orientation with respect to the load direction on the mechanical behavior of diamond unit cell. Wauthle et al. investigated both the effect of the unit cell rotation with respect to the L-PBF reference system and the sample rotation with respect to the L-PBF system with a fixed orientation of the unit cell. In both cases, the [011] oriented samples (called DIA and VER-45° in the aforementioned study) exhibit similar mechanical properties when compared with [001] ones. This result can be attributed to the poor quality of the struts produced during the L-PBF process. In fact, it is reported that the struts density was never higher than 97.5% and large pores were observed for all the samples used in the investigation. In the case of the unit cell rotation, Wauthle et al. indicated that horizontal struts should be avoided since the struts density increases with the inclination of the strut with respect to the built plate plane. Similar results on the isotropic behavior of the diamond unit cell were reported by Ahmadi et al. [36].

On the other side, the anisotropic behavior of diamond based meta-materials was reported by Soul et al. [21], partially confirming what Xie et al. [18] evaluated numerically.

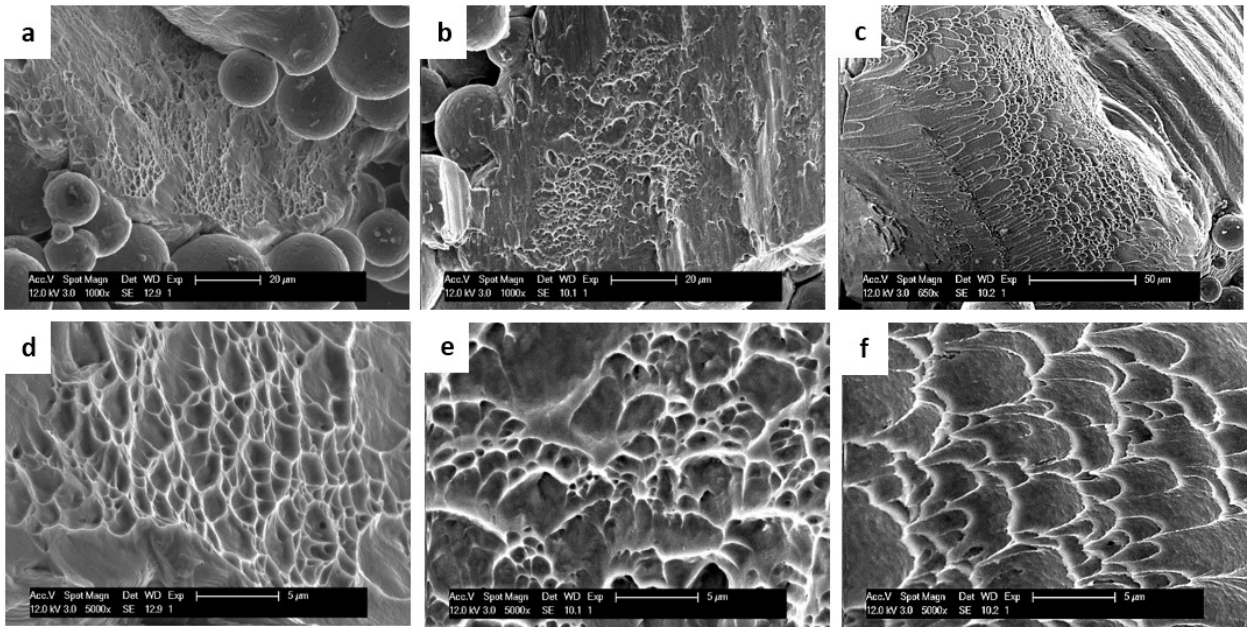

Figure 8: Representative fractured struts in HIP'ed condition for: [001] orientation (a, d); [111] orientation (b, e); [011] orientation (c, f)

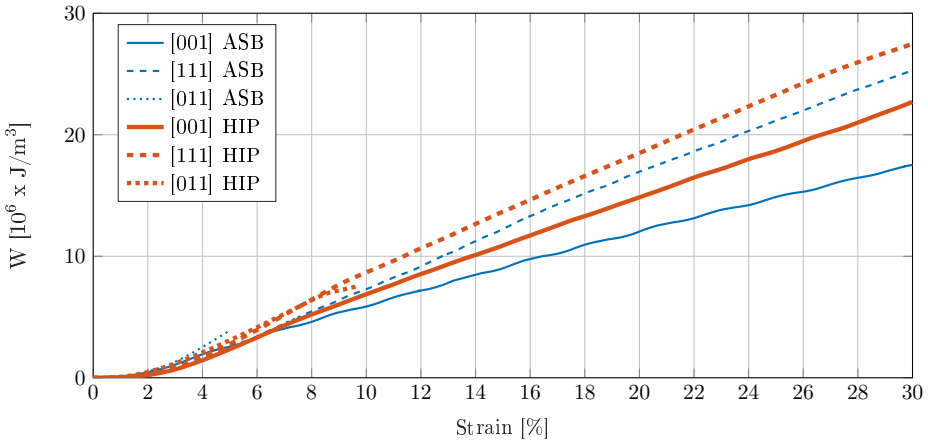

Figure 9: Cumulative energy absorption per unit volume of as-built and HIP'ed samples for different orientations

This is in line with the quasi-static tests results of the present study. The differences in quasi-elastic gradient reported in Table 1 suggest significant degree of elastic anisotropy when compared with cubic symmetry crystals, with a considerable impact of the load direction with respect to the unit cell orientation on the mechanical properties of the lattice structure.

When comparing the results of the present study with the work of Soul et al. [21], some differences in production and testing methods are to be mentioned. Soul et al. used a different material (i.e. AlMg10Si) and a different load condition, tension instead of compression. Moreover, the unit cell reference system was rotated with respect to the build plate plane (X_L, Y_L) during the production of the test specimens. As mentioned in Soul et al. study, the results obtained do not allow to assess whether the anisotropy of the diamond unit cell is mainly related to the orientation of the unit cell with respect to the load direction or to manufacturing aspects (i.e. poor consistency of struts dimensions and surface quality due to the limited L-PBF accuracy for non supported horizontal members [37]).

Despite the mentioned differences, this study presents similarities with the work of Soul et al. [21] especially as far as the failure mechanisms on macroscopic level are concerned. The three different batches present the same orientation of the slip planes as indicated by Soul et al.. The fracture patterns indicated in Table 2, 3 and 4 can be associated to the existence of weak-regions limited by planes normal to the struts directions. These weak regions exhibit the lowest resistance to global compressive forces and can be considered as the preferential directions for the slip mechanism of the structure.

To avoid inconsistency in strut quality, the samples have been manufactured fixing the unit cell orientation with respect to the L-PBF reference system. This ensures high level of consistency in dimensions and surface quality to all the struts in the unit cells of the lattice structure for all the three different batches [001], [111] and [011]. This was also confirmed by the small differences in terms of mass and relative density reported in Table 1. Moreover, since all the struts in the diamond cell have the same orientation with respect to the building direction Z_L, also the size of typical columnar grains [29] generated during the L-PBF process, can be considered similar for all the struts [38], leading to a similar microstructure across all the unit cells.

Fractography analysis of the fractured samples on microscopic level presented in Figure 7 and 8 adds more information to the redistribution of the compressive loads applied in local stresses. For [001] and [111] samples, fractured struts surfaces present equiaxed and regular dimple shapes, indicating that the main drivers for failure can be considered local tensile stresses. In case of [011] samples, the elongated dimples indicate that the failure has been mainly driven by local shear stresses.

The results collected in this investigation can be considered as design guidelines aimed to include lattice structures in load-bearing applications to achieve higher strength to weight ratios. It has been shown that changing the load orientation with respect to the unit cell affects the mechanical properties of the lattice structure. It is important to remark that the unit cell orientation has been considered fixed with respect to the build plate plane. Therefore, designers can make use of such information to optimize the orientation of the component with respect to the L-PBF

reference system to maximize the stiffness of the structure in certain directions. In addition, if the lattice structure has to be used for energy absorption applications, the current study shows that for a particular orientation of the load direction with the unit cell reference system ([011]) the porous structure presents one single and well defined fractured plane once the first peak stress is reached. After this failure, the structure ceases to absorb energy.

5. Conclusions

In this study, the influence of three different load directions with respect to the unit cell orientation on the mechanical properties of Ti-6Al-4V diamond inspired lattice structures has been investigated. The results prove that changing the load direction with respect to the unit cell orientation significantly impacts the mechanical properties and failure modes of the lattice structures, highlighting the anisotropic behavior of the diamond unit cell.

Except for the energy absorption, all the mechanical properties of the lattice structures are enhanced when the load direction changes from [001]. In particular, the quasi-elastic gradient of the [011] oriented samples ends up being 60% higher when compared to [001] oriented samples in both as-built and HIP'ed conditions. For [111] oriented samples the quasi-elastic gradient improved with 14% for as-built specimens and 33% for HIP'ed specimen with respect to [001] oriented samples. The stiffness increment generated by the reorientation of the load direction makes [011] orientation particularly attractive for achieving high strength to weight ratios for lightweight biomedical applications.

Regarding the failure modes, the three different load orientations produce three different failure patterns. The [001] oriented specimens exhibit a failure mode consisting of successive collapses of struts along planes inclined by 54.74° with respect to the horizontal plane. For the [111] oriented samples, the successive failures occur along slip planes inclined by 70.53° with respect to the horizontal plane. For this specific orientation (i.e. [111]) the energy absorption at 30% of the strain is higher in both as-built and HIP condition when compared to the energy absorption measured on [001] oriented samples. For [011] oriented specimens, the failure mechanism consists of one single collapse of struts that divides the samples in two parts. Once the failure occurs, the structure ceases to absorb energy. In this case the slip plane is inclined by 35.23° with the horizontal plane.

On a local scale, the analysis of the fractured struts via scanning electron microscope indicates that the global compressive loads redistribute in local tensile and shear stresses. For the [001] and [111] oriented specimens, post-fracture analysis indicates a dominance of the local tensile stress that produces the failure of the struts. For [011] oriented samples, the elongated dimple morphology indicates a dominance of local shear stress.

References

[1] M. Geetha, A. K. Singh, R. Asokamani, A. K. Gogia, Ti based biomaterials, the ultimate choice for orthopaedic implants–a review, Progress in materials science 54 (3) (2009) 397–425.

[2] D. Herzog, V. Seyda, E. Wycisk, C. Emmelmann, Additive manufacturing of metals, Acta Materialia 117 (2016) 371–392.

[3] A. A. Zadpoor, Mechanics of additively manufactured biomaterials (2017).

[4] J. C. M. F.R.S, L. on the calculation of the equilibrium and stiffness of frames 27 (182) 294–299. doi:10.1080/14786446408643668.
URL https://doi.org/10.1080/14786446408643668

[5] M. F. Ashby *, Hybrids to fill holes in material property space 85 (26) 3235–3257. doi:10.1080/14786430500079892.
URL https://doi.org/10.1080/14786430500079892

[6] M. Ashby, T. Evans, N. Fleck, J. Hutchinson, H. Wadley, L. Gibson, Metal Foams: a Design Guide, Elsevier.

[7] Ashby M.F, The properties of foams and lattices 364 (1838) 15–30. doi:10.1098/rsta.2005.1678.
URL https://royalsocietypublishing.org/doi/10.1098/rsta.2005.1678

[8] C. P. de Jonge, H. M. A. Kolken, A. A. Zadpoor, Non-auxetic mechanical metamaterials 12 (4) 635. doi:10.3390/ma12040635.
URL https://www.mdpi.com/1996-1944/12/4/635

[9] S. Ahmadi, S. Yavari, R. Wauthle, B. Pouran, J. Schrooten, H. Weinans, A. Zadpoor, Additively manufactured open-cell porous biomaterials made from six different space-filling unit cells: The mechanical and morphological properties 8 (4) 1871–1896. doi:10.3390/ma8041871.
URL http://www.mdpi.com/1996-1944/8/4/1871/

[10] C. Yan, L. Hao, A. Hussein, P. Young, D. Raymont, Advanced lightweight 316l stainless steel cellular lattice structures fabricated via selective laser melting 55 533–541. doi:10.1016/j.matdes.2013.10.027.
URL http://www.sciencedirect.com/science/article/pii/S0261306913009540

[11] C. Yan, L. Hao, A. Hussein, S. L. Bubb, P. Young, D. Raymont, Evaluation of light-weight AlSi10mg periodic cellular lattice structures fabricated via direct metal laser sintering 214 (4) 856–864. doi:10.1016/j.jmatprotec.2013.12.004.
URL http://www.sciencedirect.com/science/article/pii/S0924013613003804

[12] B. Van Hooreweder, Y. Apers, K. Lietaert, J.-P. Kruth, Improving the fatigue performance of porous metallic biomaterials produced by selective laser melting 47 193–202. doi:10.1016/j.actbio.2016.10.005.
URL http://www.sciencedirect.com/science/article/pii/S1742706116305232

[13] A. Cutolo, B. Neirinck, K. Lietaert, C. de Formanoir, B. Van Hooreweder, Influence of layer thickness and post-process treatments on the fatigue properties of cocr scaffolds produced by laser powder bed fusion, Additive Manufacturing 23 (2018) 498–504.
[14] G. Pyka, A. Burakowski, G. Kerckhofs, M. Moesen, S. Van Bael, J. Schrooten, M. Wevers, Surface modification of ti6al4v open porous structures produced by additive manufacturing, Advanced Engineering Materials 14 (6) (2012) 363–370.
[15] J. Kranz, D. Herzog, C. Emmelmann, Design guidelines for laser additive manufacturing of lightweight structures in TiAl6v4 27 S14001. doi:10.2351/1.4885235.
URL https://lia.scitation.org/doi/10.2351/1.4885235
[16] X. Wang, S. Xu, S. Zhou, W. Xu, M. Leary, P. Choong, M. Qian, M. Brandt, Y. M. Xie, Topological design and additive manufacturing of porous metals for bone scaffolds and orthopaedic implants: A review 83 127–141. doi:10.1016/j.biomaterials.2016.01.012.
URL http://www.sciencedirect.com/science/article/pii/S0142961216000144
[17] D. Wang, Y. Yang, R. Liu, D. Xiao, J. Sun, Study on the designing rules and processability of porous structure based on selective laser melting (SLM) 213 (10) 1734–1742. doi:10.1016/j.jmatprotec.2013.05.001.
URL http://www.sciencedirect.com/science/article/pii/S0924013613001490
[18] S. Xu, J. Shen, S. Zhou, X. Huang, Y. M. Xie, Design of lattice structures with controlled anisotropy 93 443–447. doi:10.1016/j.matdes.2016.01.007.
URL http://www.sciencedirect.com/science/article/pii/S0264127516300120
[19] G. P. Steven, Homogenization of multicomponent composite orthotropic materials using fea 13 (7) 517–531.
[20] R. Wauthle, B. Vrancken, B. Beynaerts, K. Jorissen, J. Schrooten, J.-P. Kruth, J. Van Humbeeck, Effects of build orientation and heat treatment on the microstructure and mechanical properties of selective laser melted ti6al4v lattice structures 5 77–84. doi:10.1016/j.addma.2014.12.008.
URL http://linkinghub.elsevier.com/retrieve/pii/S2214860414000323
[21] H. Soul, P. Terriault, V. Brailovski, The static and fatigue behavior of AlSiMg alloy plain, notched, and diamond lattice specimens fabricated by laser powder bed fusion 2 (2) 25. doi:10.3390/jmmp2020025.
URL http://www.mdpi.com/2504-4494/2/2/25
[22] K. Lietaert, A. Cutolo, D. Boey, B. V. Hooreweder, Fatigue life of additively manufactured ti6al4v scaffolds under tension-tension, tension-compression and compression-compression fatigue load 8 (1) 4957. doi:10.1038/s41598-018-23414-2.
URL https://www.nature.com/articles/s41598-018-23414-2
[23] E. Yasa, J. Kruth, Application of laser re-melting on selective laser melting parts 6 (4) 259–270.
[24] C. Qiu, N. J. E. Adkins, M. M. Attallah, Microstructure and tensile properties of selectively laser-melted and of HIPed laser-melted ti6al4v 578 230–239. doi:10.1016/j.msea.2013.04.099.
URL http://www.sciencedirect.com/science/article/pii/S0921509313005017
[25] B. Vrancken, L. Thijs, J.-P. Kruth, J. Van Humbeeck, Heat treatment of ti6al4v produced by selective laser melting: Microstructure and mechanical properties 541 177–185. doi:10.1016/j.jallcom.2012.07.022.
URL http://www.sciencedirect.com/science/article/pii/S0925838812011826
[26] A. Spierings, M. Schneider, R. Eggenberger, Comparison of density measurement techniques for additive manufactured metallic parts 17 (5) 380–386. doi:10.1108/13552541111156504.
URL http://www.emeraldinsight.com/doi/10.1108/13552541111156504
[27] J. A. Slotwinski, E. J. Garboczi, K. M. Hebenstreit, Porosity measurements and analysis for metal additive manufacturing process control.
URL https://www.nist.gov/publications/porosity-measurements-and-analysis-metal-additive-manufacturing-process-control
[28] ISO 13314:2011 - mechanical testing of metals – ductility testing – compression test for porous and cellular metals.
URL https://www.iso.org/standard/53669.html
[29] L. Thijs, F. Verhaeghe, T. Craeghs, J. V. Humbeeck, J.-P. Kruth, A study of the microstructural evolution during selective laser melting of ti6al4v 58 (9) 3303–3312. doi:10.1016/j.actamat.2010.02.004.
URL http://www.sciencedirect.com/science/article/pii/S135964541000090X
[30] S. J. Li, L. E. Murr, X. Y. Cheng, Z. B. Zhang, Y. L. Hao, R. Yang, F. Medina, R. B. Wicker, Compression fatigue behavior of ti6al4v mesh arrays fabricated by electron beam melting 60 (3) 793–802. doi:10.1016/j.actamat.2011.10.051.
URL http://www.sciencedirect.com/science/article/pii/S135964541100766X
[31] X. Y. Cheng, S. J. Li, L. E. Murr, Z. B. Zhang, Y. L. Hao, R. Yang, F. Medina, R. B. Wicker, Compression deformation behavior of ti6al4v alloy with cellular structures fabricated by electron beam melting 16 153–162. doi:10.1016/j.jmbbm.2012.10.005.
URL http://www.sciencedirect.com/science/article/pii/S1751616112002639
[32] Fracture analysis, in: D. M. Stefanescu (Ed.), Cast Iron Science and Technology, ASM International, pp. 399–410. doi:10.31399/asm.hb.v01a.a0006323.
URL https://dl.asminternational.org/books/book/52/chapter/641752/fracture-analysis
[33] A. Ataee, Y. Li, D. Fraser, G. Song, C. Wen, Anisotropic ti-6al-4v gyroid scaffolds manufactured by electron beam melting (EBM) for bone implant applications 137 345–354. doi:10.1016/j.matdes.2017.10.040.
URL http://www.sciencedirect.com/science/article/pii/S026412751730967X
[34] M. Zhao, F. Liu, G. Fu, D. Z. Zhang, T. Zhang, H. Zhou, Improved mechanical properties and energy absorption of BCC lattice structures with triply periodic minimal surfaces fabricated by SLM 11 (12). doi:10.3390/ma11122411.
URL https://www.ncbi.nlm.nih.gov/pmc/articles/PMC6317040/
[35] I. Maskery, N. T. Aboulkhair, A. O. Aremu, C. J. Tuck, I. A. Ashcroft, R. D. Wildman, R. J. M. Hague, A mechanical property evaluation of graded density al-si10-mg lattice structures manufactured by selective laser melting 670 264–274. doi:10.1016/j.msea.2016.06.013.
URL http://www.sciencedirect.com/science/article/pii/S092150931630658X
[36] S. Ahmadi, G. Campoli, S. A. Yavari, B. Sajadi, R. Wauthlé, J. Schrooten, H. Weinans, A. Zadpoor, Mechanical behavior of regular open-cell porous biomaterials made of diamond lattice unit cells, Journal of the mechanical behavior of biomedical materials 34 (2014) 106–115.
[37] T. Craeghs, S. Clijsters, E. Yasa, F. Bechmann, S. Berumen, J.-P. Kruth, Determination of geometrical factors in layerwise laser melting using optical process monitoring, Optics and Lasers in Engineering 49 (12) (2011) 1440–1446.

[38] V. Weißmann, R. Bader, H. Hansmann, N. Laufer, Influence of the structural orientation on the mechanical properties of selective laser melted ti6al4v open-porous scaffolds, Materials & Design 95 (2016) 188–197.